Polymer 50 (2009) 1095–1102

Contents lists available at ScienceDirect

Polymer

journal homepage: www.elsevier.com/locate/polymer

Crosslinking in metallocene ethylene-*co*-5,7-dimethylocta-1,6-diene copolymers initiated by electron-beam irradiation

María L. Cerrada [a,*], Rosario Benavente [a], Marta Fernández-García [a], Ernesto Pérez [a], João M. Campos [b], M. Rosário Ribeiro [b]

[a] *Instituto de Ciencia y Tecnología de Polímeros (CSIC), Juan de la Cierva 3, 28006 Madrid, Spain*
[b] *Instituto de Ciência e Engenharia de Materiais e Superfícies – ICEMS, Instituto Superior Técnico – IST, Departamento de Engenharia Química e Biológica, Universidade Técnica de Lisboa – UTL, Av. Rovisco Pais, 1049-001 Lisboa, Portugal*

ARTICLE INFO

Article history:
Received 6 August 2008
Received in revised form
22 December 2008
Accepted 7 January 2009
Available online 14 January 2009

Keywords:
Ethylene-*co*-5,7-dimethylocta-1,6-diene copolymers
Electron-beam irradiation
Gel content

ABSTRACT

The synthesis of ethylene-*co*-5,7-dimethylocta-1,6-diene copolymers (CEDMO) with different molar DMO contents has been performed to incorporate double bonds in the lateral and make easier the development of crosslinkings in the resulting polymer material after application of electron-beam irradiation. The gel content as well as a comprehensive evaluation of the changes in the crystalline characteristics have been carried out. Both features are strongly dependent on DMO composition and irradiation doses. Variation in the mechanical response of the different specimens has been checked by microhardness measurements.

1. Introduction

Crosslinking is a broadly used method for the modification of polymer properties. This process involves the formation of tridimensional structures causing substantial changes. Crosslinked polyolefins, especially PE, are of significant practical interest as well as crosslinked rubbers and thermosetting resins. All commercially utilised processes for the initiation of polyolefin crosslinking are based on the formation of polyalkene macroradicals at some stage of the process. Common ways of initiating crosslinking involve macroradical formation via thermal decomposition of organic peroxides [1], high energy irradiation (gamma or electron beam) [2–4] and grafting of silane groups, which form crosslinks via hydrolysis of silanole moieties [5]. Other procedures for initiation of polyolefin crosslinking are less frequently used or have only been investigated in the laboratory. These include high-frequency heating, initiation by thermal decomposition of azo-esters or ethers, UV irradiation, redox initiation and free radical initiated grafting of various moieties onto polyalkene chains which can react under various conditions leading to the formation of crosslinks often physical or physico-chemical in nature [6]. Several interesting modifications of peroxide initiated crosslinking were suggested. A detailed description of the various initiation procedures together with mechanisms for these processes and specific features of each procedure was given in a comprehensive review by Lazar et al. [7]

Polyethylene, PE, is reported to be widely used in medical devices and pharmaceutical packaging [8]. Each type (high density, HDPE, low density, LDPE and linear low density, LLDPE) offers different benefits and **functionalities**: HDPE provides stiffness, chemical resistance and barrier properties while LDPE offers resistance to stress cracking and excellent impact properties. In addition, its capability of being sterilized is a favourable and an important aspect. The objective of sterilization is to prevent the introduction of pathogenic organisms **into the body**. Sterilization can be achieved through a variety of methodologies, the electron-beam irradiation being commonly utilized. As aforementioned, upon irradiation PE predominantly undergoes crosslinking in the amorphous regions or at the boundaries of crystallites [6]. The crosslinking takes place in the solid state and changes its morphological characteristics and, accordingly, its mechanical properties at ambient temperature. This variation on the mechanical behaviour depends very much on the type of PE, molecular weight, processing and crosslinking conditions, and other factors, irradiation dose being one of the most important parameters.

* Corresponding author. Instituto de Ciencia y Tecnología de Polímeros (CSIC), Chemical Physics Department, Juan de la Cierva 3, 28006 Madrid, Spain. Tel.: +34 91 5622900; fax: +34 91 5644853.
E-mail address: mlcerrada@ictp.csic.es (M.L. Cerrada).

0032-3861/$ – see front matter © 2009 Elsevier Ltd. All rights reserved.
doi:10.1016/j.polymer.2009.01.006

Moreover, **functional** monomers, such as multifunctional acrylate, methacrylate and allylic reactive molecules, can be additionally blended with the base PE to promote crosslinking at a reduced radiation level [1]. **A decrease of the degree of crystallinity can be observed when crystallisation** proceeds from a crosslinked melt.

The current investigation is focused on another strategy, not explored up to now to the best of our knowledge, and aims to facilitate the development of crosslinking in PE based samples. This approach consists of the preparation of unsaturated polyolefins through the copolymerisation of ethylene with non-conjugated dienes. This synthetic route takes advantage of the use of metallocene catalysts [9–13] leading to the synthesis of copolymers with narrow molecular weight distributions and with the side branches randomly distributed along the polymer backbone. 5,7-Dimethyl-1,6-octadiene was chosen as comonomer since it has a vinylic double bond that can be polymerised with a metallocene catalyst, while the presence of substituents on the second double bond inhibits its polymerisation leading this way to pendant double bonds on the ethylene-*co*-5,7-dimethylocta-1,6-diene copolymers.

Therefore, the goals of this research are, on one hand, the synthesis of ethylene-*co*-5,7-dimethyl-1,6-octadiene copolymers (CEDMO) with pendant unsaturations in low molar composition to avoid a significant loss of crystallinity [14] and, on the other hand, the further evaluation of the effect of different irradiation doses on their structure and the mechanical behaviour, comparing the results with those found in an also metallocene HDPE. The structural changes have been checked by wide and small angle X-ray scattering, WAXS and SAXS respectively, Fourier transform infrared spectroscopy, FTIR, and differential scanning calorimetry, DSC, whereas microhardness measurements have been performed as starting point in evaluating the mechanical response.

2. Experimental part

2.1. Polymerisations

Methylaluminoxane, MAO (*Witco*), was purchased as a 10% (m/v) toluene solution. $Me_2Si(Cp)(Flu)ZrCl_2$ (Boulder), methanol and HCl (*Merck*) were used as received. Toluene (*Petrogal*), 5,7-dimethylocta-1,6-diene (*DRT*), nitrogen and ethylene (*Air Liquide*) were purified according to standard procedures.

The ethylene-*co*-5,7-dimethyl-1,6-octadiene copolymers were synthesised using a metallocene catalyst $Me_2Si(Cp)(Flu)ZrCl_2$ in association with MAO at several comonomer compositions. Polymerisations were performed in a 1.0 dm^3 magnetically stirred Büchi autoclave at room temperature and 1.1 bar ethylene pressure. Toluene, ethylene and the comonomer were charged into the reactor. Catalyst ($[Zr] = 2 \times 10^{-4}$ M) was separately pre-contacted with MAO for 15 min. The polymerisation started with the introduction of the pre-activated catalyst; an aluminium to **zirconium** molar ratio of 1000 was used. After 30 min, **the polymerisation mixtures were precipitated over methanol acidified with HCl, and the polymeric powder attained was further filtered and washed two times with fresh methanol before drying.**

Several ethylene-*co*-5,7-dimethylocta-1,6-diene copolymers, with different comonomer content, were obtained. They were labelled as CEDMO followed by two numbers that indicate their molar composition in DMO (see Table 1). The HDPE homopolymer analysed was similarly named as CEDMO0.0.

2.2. Polymer characterisation

The formation of ethylene-*co*-5,7-DMO copolymers was investigated by FTIR and ^{13}C NMR techniques. An initial infrared analysis allowed the observation of an absorption at 840 cm^{-1}, characteristic of the C–H vibration in the 5,7-DMO substituted double bond, indicating that the dimethyl substituted vinyl unsaturation remains untouched after copolymerisation. The ^{13}C NMR identification of the peaks corresponding to the branching methine carbon (38.4 ppm) and to the methylenic carbons α and β (34.6 and 27.3 ppm, respectively), as well as some other peaks characteristic of 5,7-DMO, confirms the formation of ethylene/5,7-DMO copolymers. We could not identify structures due to diene cyclisation reactions and the carbon and proton NMR spectra show the presence of the 5,7-DMO substituted double bond in the formed copolymers. Copolymer compositions were calculated from their ^1H NMR spectra and according to peak assignment already reported in literature [12,15].

Table 1
Crystallinity values at room temperature determined from the WAXS profiles represented in Fig. 5.

Specimen	DMO content (mol %)	Irradiation dose				
		NR	*A*	*B*	*C*	*D*
CEDMO0.0	0.0	0.62	0.60	0.62	0.61	0.61
CEDMO0.7	0.7	0.42	0.42	0.40	0.41	0.41
CEDMO1.0	1.0	0.39	0.40	0.40	0.40	0.41
CEDMO1.9	1.9	0.39	0.40	0.39	0.39	0.39

2.3. Preparation of specimens

The different CEDMO copolymers and the corresponding homopolymer analysed in the current paper were obtained as **films** by compression moulding in a Collin press between hot plates (150 °C) at a pressure of 1.5 MPa for 5 min for their structural characterization and analysis of their mechanical response by microhardness. **Thickness ranged from 500 to 550 μm.** Each one of the CEDMO samples was crystallized by a fast quench between plates cooled with water after its melting in the press.

2.4. Irradiation of specimens

Electron-beam (EB) irradiation was carried out at IONMED (an industrial installation) in atmospheric air at ambient temperature using a 10 MeV Rhodotron accelerator. All polymeric films were irradiated on one side using a current of 5 mA such that the polymeric samples were exposed to an irradiation dose of about 33.3 kGy per pass. Several passes under these conditions were required for high irradiation doses. The EB irradiation doses are ranged throughout this work from 33 to 233 kGy. A label related to identification of the dose applied is added to the name of each copolymer. Therefore, **NR represents non-irradiated samples and *A*, *B*, *C* and *D* upper cases indicate the dose: 33, 67, 133 and 233 kGy, respectively**.

2.5. Gel content determination

The gel content **(insoluble fraction)** of the different specimens was determined gravimetrically, according to ASTM D 2765, using a 16-h Soxhlet extraction cycle, with *p*-xylene as the solvent at 140 °C. The polymeric samples were cut into small pieces and placed in a pre-weighed stainless steel, fine wire mesh. After the extraction cycle, the samples were washed with acetone and vacuum-dried to a constant weight. **The gel content was calculated as the percentage ratio of the final weight of the insoluble polymeric fraction to its initial weight previous extraction** [1].

2.6. X-ray scattering measurements

The synchrotron studies were performed in the soft-condensed matter beamline A2 at Hasylab (Hamburg, Germany), working at a wavelength of 0.150 nm. The experimental setup includes a heating chamber specimen holder, a MARCCD detector for acquiring SAXS patterns (sample-to-detector distance being 260 cm) and a linear detector for WAXS measurements (distance 21 cm). All experiments comprise the heating of samples from 26 up to 158 °C at 12 °C/min. The data acquisition was done in frames of 10 s. A sample of crystalline PET sample was used for WAXS calibration and the different orders of the long spacing of rat-tail cornea ($L = 65$ nm) were utilized for the SAXS detector. The two-dimensional X-ray patterns from the MARCCD detector were processed with the FIT2D program of Dr. Hammersley (ESRF) and converted into one-dimensional arrays after normalization for the intensity of the primary beam and subtraction of the scattering of an empty sample **(aluminium foil envelope)**.

2.7. Fourier transform infrared spectroscopy

The IR spectra were obtained on films using a Perkin-Elmer FTIR spectrometer equipped with an ATR device scanning between 600 and 4000 cm^{-1}; 4 scans were accumulated for each specimen at a resolution of 4 cm^{-1}.

2.8. Differential scanning calorimetry

Calorimetric analyses were carried out in a Perkin-Elmer DSC7 calorimeter, connected to a cooling system and calibrated with different standards. The sample weights ranged from 6 to 7.5 mg. A temperature interval from −50 °C to 150 °C has been studied and the used heating rate was 10 °C/min. For crystallinity determinations, a value of 290 J/g has been taken as the enthalpy of fusion of a perfectly crystalline material [16,17].

2.9. Microhardness determination

A Vickers indentor attached to a Leitz microhardness tester was used to perform microindentation measurements undertaken at 23 °C. A contact load of 0.98 N and a contact time of 25 s were employed. Microhardness, MH, values (in MPa) were calculated according to the relationship [18]:

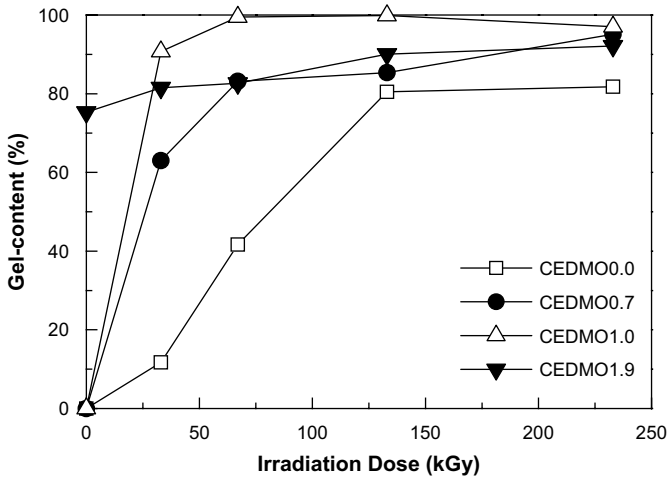

Fig. 1. Effect of irradiation dose on the gel content of crosslinked polyethylene, CEDMO0.0, and its copolymers with different DMO contents.

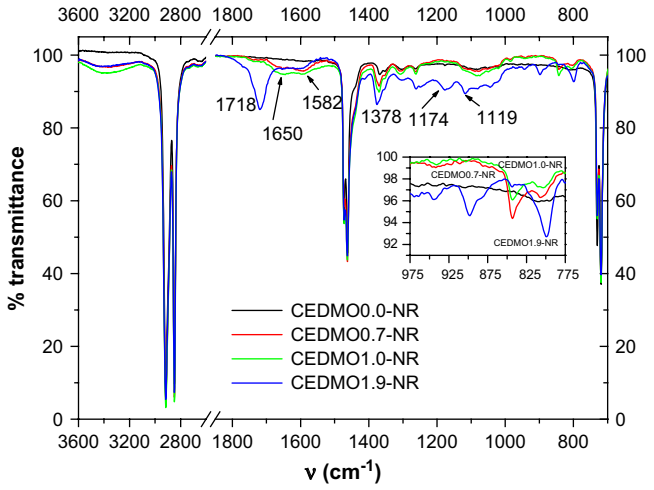

Fig. 2. FTIR absorption spectra at room temperature for the different non-irradiated specimens.

$$\mathrm{MH} = 2\sin 68^{\circ} P/d^2 \quad (1)$$

where P (in N) is the contact load and d (in mm) is the diagonal length of the projected indentation area. Diagonals were measured in the reflected light mode within 30 s of load removal, using a digital eyepiece equipped with a Leitz computer-counter-printer (RZA-DO).

3. Results and discussion

Fig. 1 shows the gel content of the specimens, CEDMO0.0 homopolymer and the respective copolymers, versus irradiation dose. The extent of gel formation in the exposed samples is strongly dependent on DMO composition and irradiation dose. Higher gel content corresponds to a higher portion of the network structure in the amorphous region of the polymer, which is insoluble in the solvent. The sol content is related to the **non-crosslinked** portion of the polymer in both amorphous and crystalline regions. It should be noted that the crystalline portion of the polymer is soluble in *p*-xylene at 140 °C, which is inferred from the zero gel content of non-crosslinked specimens. It is seen, however, that CEDMO1.9 copolymer exhibits important gel content even in the non-irradiated specimen, CEDMO1.9-NR. This fact is ascribed to the easiness exhibited by double bonds to promote crosslinkings in this

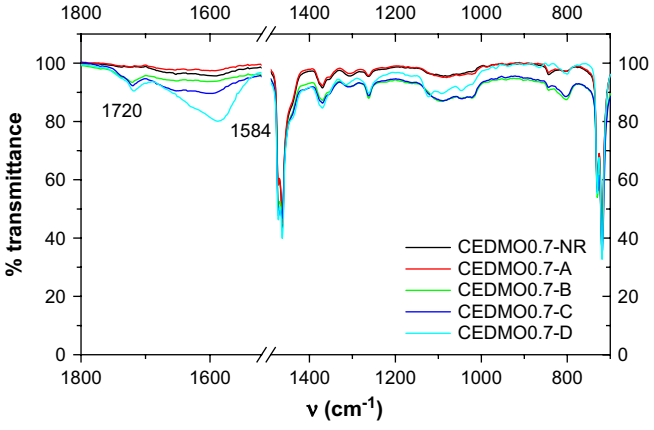

Fig. 3. FTIR absorption spectra at room temperature for CEDMO0.7 specimens non-irradiated and irradiated at the distinct doses.

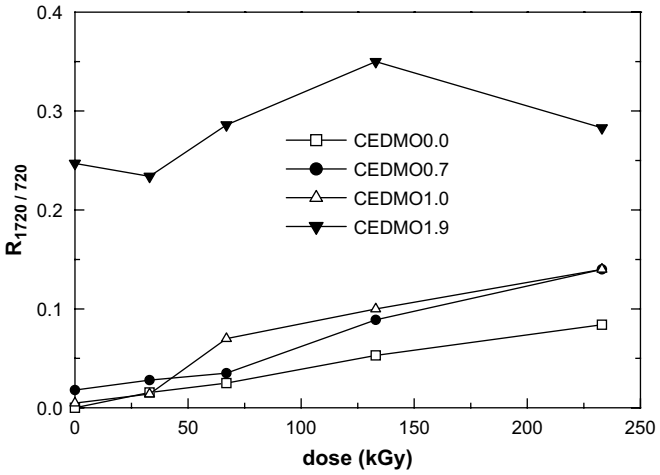

Fig. 4. Ratio of absorbance at 1720 cm^{-1} band to that found at 720 cm^{-1} for the samples under study irradiated at different doses.

copolymer with the highest DMO content. This initial crosslinking, accompanied by beginning of double bonds oxidation, as will be discussed in FTIR results, has been generated from the powdered specimen after its synthesis by simple stay at room temperature for several months without any processing. In addition, its extent can be enlarged during its processing at 150 °C (see its FTIR spectrum in Fig. 2).

The other two non-irradiated copolymers, CEDMO0.7-NR and CEDMO1.0-NR, present zero gel content as well as the homopolymer CEDMO0.0-NR **in spite of all of them were prepared at the same time and, consequently, stayed identical period of time before being processed and irradiated.**. Therefore, the effect of composition is rather significant when electron irradiation is applied. Thus, the crosslinking level in the CEDMO0.0 homopolymer gradually increases at the smaller doses up to reach a maximum value of around 80% (see Fig. 1). Incorporation of the DMO comonomer, even in a molar fraction as low as 0.7, leads to a significant increase of gel content at the smallest doses: around five times in CEDMO0.7-A compared with CEDMO0.0-A and about the double in CEDMO0.7-B respect to CEDMO0.0-B. The maximum value attained is also higher: 90% versus 80% in the CEDMO0.0-D homopolymer. A slightly higher DMO addition leads to the almost complete crosslinking content at 67 kGy, the crosslinking level at 33 kGy being around 90%. Consequently, the incorporation of DMO significantly changes the gel content mainly for the smaller irradiation dose, generally used in the standard applications: the typical sterilization dose is around 25–30 kGy.

The changes in the network structure of the different polymeric materials analysed are observed in Figs. 2 and 3. The former represents the FTIR spectra found in films of the non-irradiated specimens. The CEDMO0.0-NR homopolymer spectrum does not exhibit any bands at wavenumber higher than 3000 cm^{-1} and within the 1500–2700 cm^{-1} interval, as characteristic of a saturated hydrocarbon [19]. In addition, CEDMO0.0-NR specimen shows four strong IR absorption peaks corresponding to stretching (at 2847 and 2917 cm^{-1}), deformation (around 1463 cm^{-1}) and rocking vibrations (at 720 cm^{-1}) of methylene groups and to symmetric deformation vibration of methyl units at 1378 cm^{-1}.

Some changes are observed in the spectra as DMO comonomer is incorporated in the different copolymers. The band at 1378 cm^{-1}, which provides information about the existence of branching, increases its intensity as DMO content does. In addition, CEDMO0.7-NR and CEDMO1.0-NR exhibit weak vibrations in the C=C stretching band region, at around 1600 cm^{-1} due to the incorporation of DMO counits and to some terminal unsaturated groups. However, in CEDMO1.9-NR the intensity of these bands appears partially overlapped to other one in the range 1735–

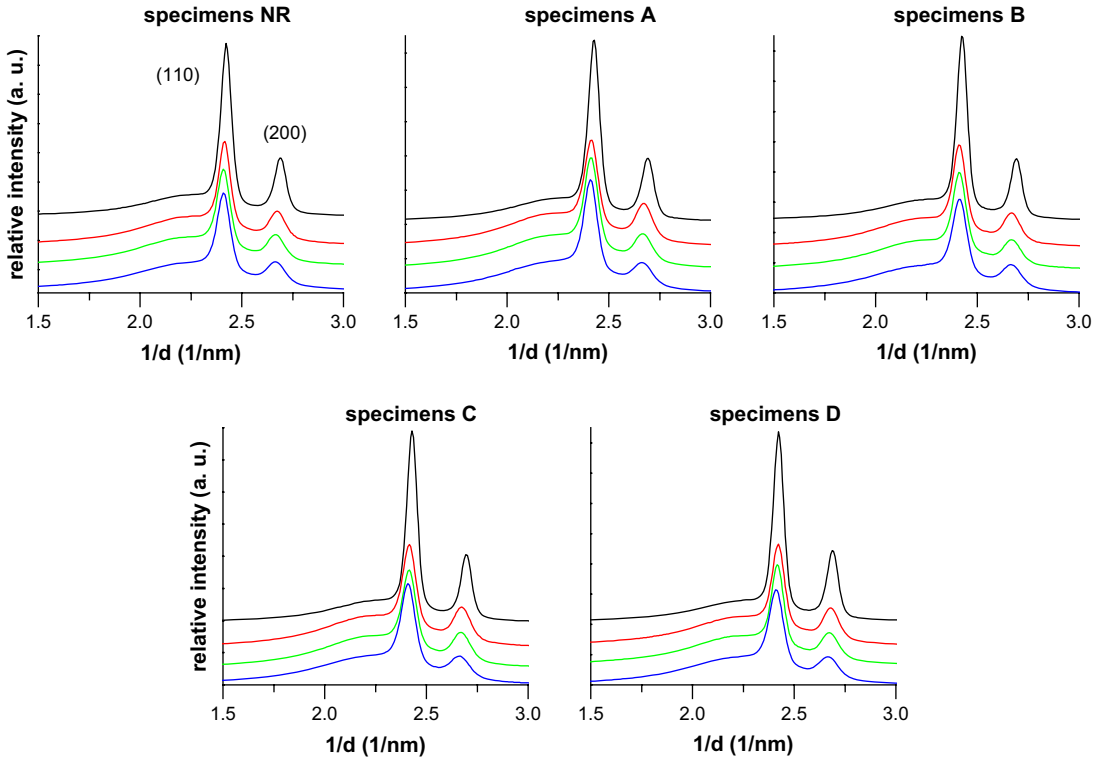

Fig. 5. WAXS patterns, at room temperature, for the samples non-irradiated and irradiated at different doses. Specimens are in each plot from top to bottom: CEDMO0.0, CEDMO0.7, CEDMO1.0 and CEDMO1.9, respectively.

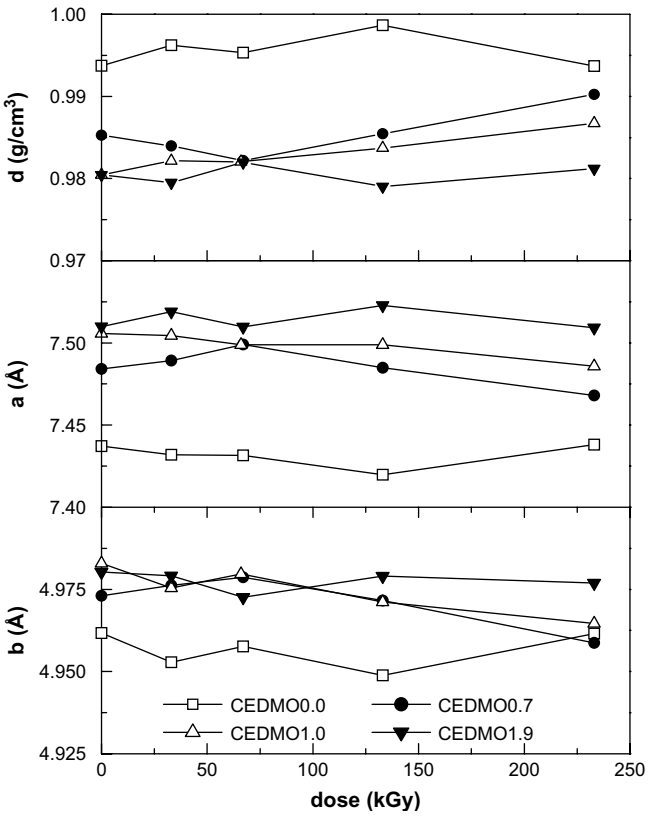

Fig. 6. Variation with irradiation dose of the orthorhombic lattice characteristics (crystal density (*d*) and *a* and *b* axes).

1700 cm^{-1} ascribed to C═O vibrations. Additional bands also develop in the characteristic region of C–O vibrations (1050–1170 cm^{-1}). The simple maintenance at oxidative atmosphere existing at ambient conditions and further processing of this CEDMO1.9 copolymer leads to the oxidation of some double bonds and, consequently, the appearance of these characteristic C═O and C–O vibration bands. On the other hand, all of the CEDMO copolymers exhibit a wide band ranged from 3200 to 3500 cm^{-1} associated with the O–H stretching vibration and probably connected to the formation of some hydroperoxides (3400 cm^{-1} region). In agreement with the gel content determination (Fig. 1) a marked decrease of the intensity of the C–H vibration in the 5,7-DMO substituted double bond, at 840 cm^{-1}, is observed for CEDMO1.9-NR. New bands are seen at 890 cm^{-1} (vinylidene region) and at 800 cm^{-1} (see inset in Fig. 2).

Fig. 3 depicts the effect of irradiation dose found in the CEDMO0.7 copolymer. As expected the 840 cm^{-1} band almost disappears for the sample exhibiting the highest gel content CEDMO0.7-D. There is **no** evidence of the C═O band in the CEDMO0.7-NR and CEDMO0.7-A specimens whereas a small vibration is observed in this interval in the samples irradiated with higher dose, indicating that oxidation starts although in a small extent. The bands in the characteristic region of C–O and O–H vibrations are also increased for the higher radiation doses. Moreover, an increase of intensity is seen in the bands at about 1580 cm^{-1} and 1470 cm^{-1} as irradiation dose is enlarged.

The increase of irradiation doses modifies the gel content for the different specimens, as depicted in Fig. 1, and leads, together with oxidative atmosphere existing at ambient, to the beginning of decomposition processes, as previously shown. To learn about the extent of this degradation, Fig. 4 represents the ratio between the bands at 1720 and 720 cm^{-1}, related to stretching vibration of carbonyl groups (ketones, lactones and peroxides among others) and the one at 720 associated with rocking CH_2 band taken as reference. It can be deduced that degradation significantly increases as irradiation dose does and it is more important as DMO molar fraction is enlarged in the copolymer. The behaviour of CEDM1.9 is rather different, as previously observed also from gel content determination. The oxygen existing in the environment is enough to initiate the oxidation of double bonds because of its relatively high content.

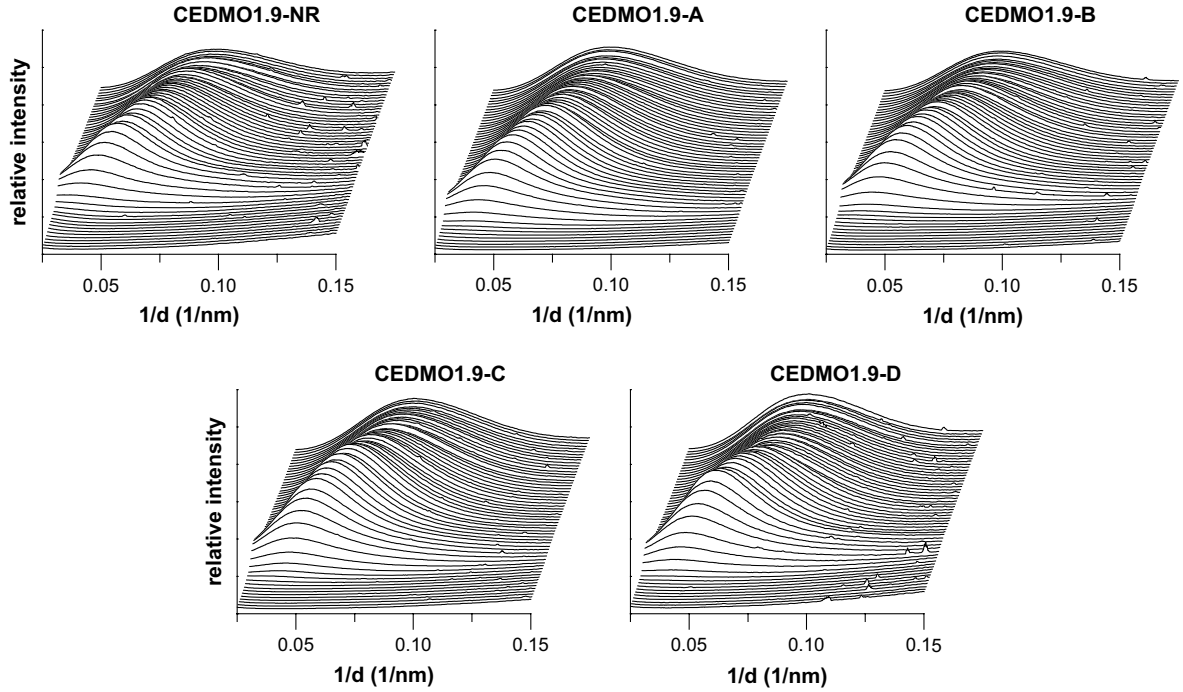

Fig. 7. Real-time SAXS profiles, obtained with synchrotron radiation for the copolymer CEDMO1.9 non-irradiated and irradiated at different doses in melting experiments at 12 °C/min.

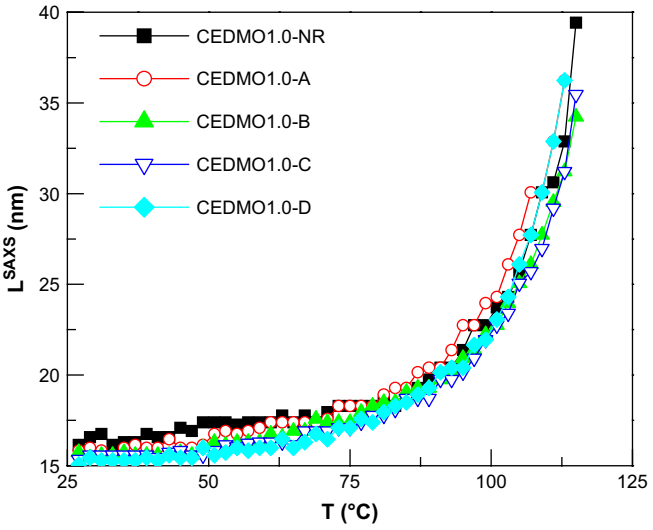

Fig. 8. Effect of temperature on the Lorentz-corrected long spacing during the melting experiments for the CEDMO1.0 non-irradiated and irradiated specimens.

Consequently, degradation in CEDMO1.9-NR starts even before irradiation, as well as crosslinking.

Fig. 5 points out that all of the non-irradiated samples are semicrystalline in spite of the microstructural changes just mentioned. Accordingly, the WAXS profiles exhibit the common (110) and (200) diffraction peaks characteristic for the polyethylene orthorhombic lattice [20,21]. The DMO units copolymerised with ethylene in the present work are rather bulky and, therefore, the capability of being incorporated to the PE crystalline lattice does not practically exist. Consequently, they impose a high hindrance for the PE crystallisation and a considerable decrease in the (110) and (200) diffraction intensities is observed as DMO content increases in the copolymer since the average number of consecutive ethylene units decreases and, accordingly, the crystallisable part becomes smaller. In addition to this diminishment in crystallinity (see values in Table 1), a shift of the positions of the maxima to lower angles is observed, indicating that the basal *a*–*b* plane of the orthorhombic unit cell expands and the corresponding spacings, d_{110} and d_{200}, increase with DMO content. Consequently, a higher distortion of the orthorhombic crystalline lattice is exhibited. Moreover, the crystalline diffractions are broadened, pointing also out a decrease in the crystallites size with the increase of DMO content. SAXS results corroborate this assumption, as will be discussed later on.

The orthorhombic lattice constants can be determined from the d_{110} and d_{200} spacings. They show a clear dependence upon the copolymer composition in the non-irradiated specimens, as depicted in Fig. 6. The *a* axis is more dependent on composition than the *b* one, though both of them increase as DMO content is raised. Once these two axes are known, the density of the corresponding crystal can be determined, assuming a value of 2.54 Å for the *c* axis. As expected, the density decreases as DMO content is increased in the polymer. In relation to the influence of irradiation dose, an opposite dependence is found between the homopolymer and the copolymers. In the CEDMO0.0, density is the smallest at the highest dose compared to those found at lower doses, while in the copolymers the observed trend points out to an increase in crystal density as dose is raised.

To get a deeper insight about structural changes, real-time variable-temperature experiments employing synchrotron radiation were performed in the small angle region, as represented in Fig. 7 for the CEDMO1.9 copolymer at the different doses. The existence of long spacing is exhibited in the different plots and is attributed to the presence of lamellar crystals. The analysis of the different profiles as a function of temperature allows obtaining information about the structure variation during melting in these samples. At a given specimen and dose (Fig. 7), the location of SAXS maxima slightly moves to lower values of $1/d$, meaning that the most probable long spacing, $L^{SAxS} = d_{max}$, deduced from the Lorentz-corrected SAXS profiles, increases with temperature until its disappearance in the molten state. This fact can be more clearly seen in Fig. 8, where L^{SAxS} is explicitly depicted for the different CEDMO1.0 specimens. Three regions can be observed: an initial one, up to around 60 °C, where the L^{SAxS} is almost constant; a second region, between 60 °C and around 90 °C, with a moderate increase of L^{SAxS}; and a final one, with a very important thickening process. This last region is ascribed to the usual melting–recrystallisation phenomena. Therefore, the increase of temperature leads to an improvement of crystallites and they become somewhat larger and thicker. These results are rather similar for all of the copolymers, with some minor differences: the initial long spacings

Table 2
Most probable long spacing (L^{SAxS}, nm) and **crystallite size** (l_c^{SAxS}, nm) at room temperature determined from SAXS profiles.

Specimen	L^{SAxS} (nm)					l_c^{SAxS} (nm)				
	Irradiation dose					**Irradiation dose**				
	NR	*A*	*B*	*C*	*D*	**NR**	***A***	***B***	***C***	***D***
CEDMO0.0	28.6	28.2	28.5	28.2	27.5	**17.7**	**16.9**	**17.1**	**17.2**	**16.8**
CEDMO0.7	16.4	16.7	16.1	15.9	15.9	**6.9**	**7.0**	**6.5**	**6.5**	**6.5**
CEDMO1.0	16.3	15.6	15.5	15.4	15.2	**6.4**	**6.3**	**6.2**	**6.2**	**6.2**
CEDMO1.9	13.3	13.3	13.4	13.1	13.1	**5.2**	**5.2**	**5.2**	**5.1**	**5.1**

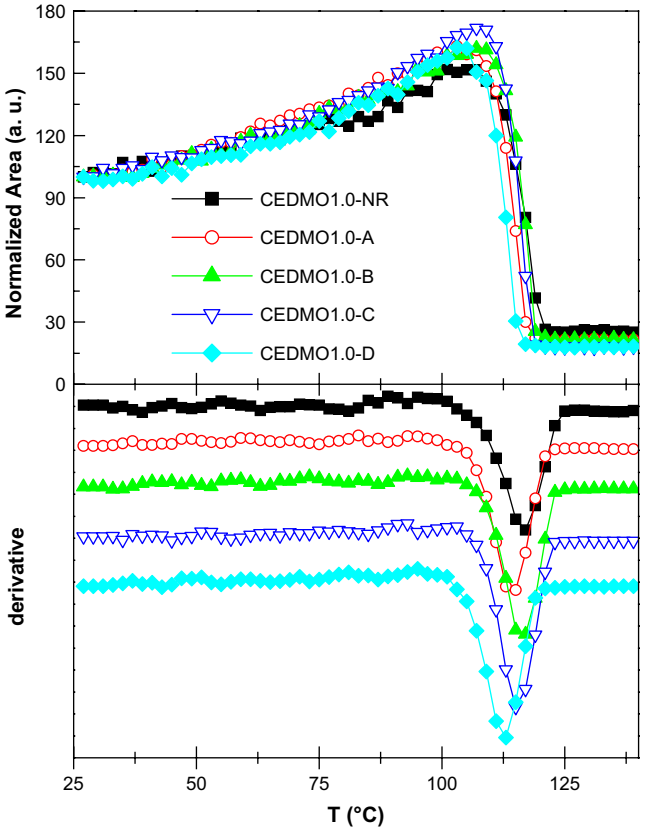

Fig. 9. Temperature dependence of either relative SAXS invariant (top plot) or SAXS invariant derivative (bottom plot) for the different CEDMO1.0 specimens during melting experiments.

Table 3
Melting temperatures determined by DSC (T_{m1}^{DSC} and T_{m2}^{DSC}, **determined from the first and second heating run respectively**) and real-time temperature-variable SAXS (T_m^{SAxS}) experiments.

Specimen	Irradiation dose														
	NR			*A*			*B*			*C*			*D*		
	T_{m1}^{DSC}	T_m^{SAxS}	$\mathbf{T_{m2}^{DSC}}$	T_m^{DSC}	T_m^{SAxS}	$\mathbf{T_{m2}^{DSC}}$	T_m^{DSC}	T_m^{SAxS}	$\mathbf{T_{m2}^{DSC}}$	T_m^{DSC}	T_m^{SAxS}	$\mathbf{T_{m2}^{DSC}}$	T_m^{DSC}	T_m^{SAxS}	$\mathbf{T_{m2}^{DSC}}$
CEDMO0.0	133	136	**134**	132	134	**132**	132	137	**131**	131	137	**129**	131	133	**127**
CEDMO0.7	114	115	**113**	114	116	**111**	113	114	**110**	113	115	**110**	113	116	**110**
CEDMO1.0	111	115	**111**	110	114	**108**	110	116	**107**	111	115	**107**	111	113	**107**
CEDMO1.9	105	107	**104**	104	109	**103**	104	109	**102**	105	111	**102**	104	111	**101**

are somewhat lower than those found in the CEDMO0.0 homopolymer and slightly dependent on composition (see Table 2) and the final thickening region occurs at lower temperatures, as correspond to lower melting temperatures. The irradiation leads to a reduction of L^{SAxS} values, this diminution exhibiting a less extent in the CEDMO1.9 copolymer. This feature might be associated with the smaller variation that amorphous regions surrounding crystallites undergo since the initial CEDMO1.9-NR present a gel content similar to that found in the CEDMO1.9-D specimen.

Additional information can be obtained from the analysis of the relative SAXS invariant [22,23]. The temperature evolution of this invariant for the different CEDMO1.0 specimens is shown in the upper part of Fig. 9. It can be observed that, after an initial region of very small increase of the invariant, it follows a more considerable increase, before the final sharp decrease during melting, similar to the different stages discussed for temperature-variable L^{SAxS} values. The lower part of Fig. 9 shows the corresponding derivatives of the relative invariant. These derivatives provide values of melting temperatures that correlate well with those obtained from DSC experiments, as reported in Table 3.

Crosslinking has taken place in solid state for the polymers under study. Therefore, radiation mainly has affected the amorphous phase while the crystalline phase has remained rather intact (see values of crystallinity and most probable crystal size in Tables 1 and 2) and T_m values do not practically change during the first heating process at a given specimen. However, a dependence on DMO content has been observed, as expected. The DSC runs of the subsequent cooling and heating processes were performed to learn more on the effect of irradiation in these materials. At a given sample, T_m values found in the second heating processes are lowered compared with those observed during the first one as much as irradiation dose increases. That means that once the isotropic amorphous phase is reached and the subsequent cooling to an ambient temperature is performed the crosslink junctions play a role and crystallite development is hindered.

The knowledge of L^{SAxS} and the total WAXS crystallinity at room temperature for the different specimens at the distinct irradiation doses allows estimating the most probable crystallite size in the direction normal to the lamellae, l_c, by assuming a simple two-phase model. The results for l_c are listed in Table 2. Again, the l_c crystal size is more dependent on composition than on irradiation. Therefore, l_c values decrease as DMO content and irradiation doses increase, this latest effect being more significant for the high doses.

The effect of both copolymerisation and irradiation dose on the mechanical response has been evaluated by performing microhardness measurements. Fig. 10 displays the microhardness results found for the different specimens at the distinct irradiation doses as preliminary investigation of the effect in the mechanical behaviour of these polymeric materials. MH measures primarily the resistance of the material to plastic deformation and, accordingly, provides an idea about local strain. Several effects can be distinguished along microhardness measurements in semicrystalline polymers [18]: an elastic deformation that yields an instant elastic recovery on unloading; a permanent plastic deformation determined by arrangement and structure of crystallites and their connection by tie molecules and entanglements; and a time-dependent MH during loading and a long delayed recovery after load removal (viscoelastic contribution). Therefore, though MH measurements are related to the superficial mechanical response they also involve a complex combination of other bulk mechanical properties (elastic modulus, yield strength, strain hardening, toughness). Hence, a direct correlation with rigidity modulus is commonly found [14,24,25].

It is observed in Fig. 10 that microhardness decreases in the non-irradiated specimens as DMO content increases, as seen by comparison between values found in CEDMO0.0-NR, CEDMO0.7-NR and CEDMO1.0-NR. However, this effect with composition is not evident if MH results between CEDMO1.0-NR and CEDMO1.9-NR are evaluated since values are 13.7 and 14.0 MPa respectively. Crystallinity is similar in both specimens (see Table 1) and the most probable crystallite size in the direction normal to the lamellae, l_c, is higher **in CEDMO1.0-NR** than in CEDMO1.9-NR (see Table 2). Therefore, rigidity measured by MH could be expected to be higher in CEDMO1.0-NR. Nevertheless, an important difference exists between these two samples. The gel content, *i.e.*, the amount of chains crosslinked is rather different: 0 for CEDMO1.0-NR and close to 80% in CEDMO1.9-NR. This crosslinking percentage has not significantly influenced the characteristics of crystalline regions, composition being the most important parameter. However, the bulk of specimens is essential for their mechanical response. Therefore, the existence of a highly crosslinked amorphous phase in CEDMO1.9-NR allows it to overcome its crystalline handicap derived from its sensibly higher composition in DMO comonomer.

The importance of the presence of crosslinkings is evident from the MH results exhibited by CEDMO0.0 at the different irradiation

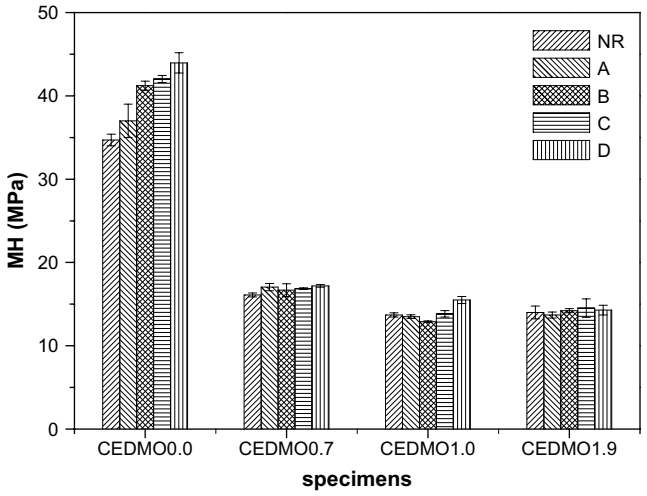

Fig. 10. Variation of the microhardness (MH) as function of irradiation doses for the different polymeric materials analysed: CEDMO0.0, CEDMO0.7, CEDMO1.0 and CEDMO1.9 from left to right.

doses. Crystallinity is rather constant with doses while L^{SAxS} and, consequently, l_c values slightly diminish. The progressive enlargement of the gel content, up to a maximum value close to 80%, leads to an increase of its rigidity and, accordingly, of its MH. The effect of irradiation in CEDMO0.7 and CEDMO1.0 is not as positive as in CEDMO0.0. The incorporation of DMO as comonomer is relatively low in both polymeric materials but its presence significantly reduces the crystallites content, the more rigid component, therefore, MH decreases compared to that found in CEDMO0.0 at the different doses. The high crosslinking level associated with irradiation leads to slightly higher MH values in both copolymers. On the other hand, the irradiation doses seem not to alter the rigidity of CEDMO1.9 due probably to its initial high crosslinking level (close to 80%) and, consequently, the small changes derived from irradiation in its crystalline and amorphous regions.

4. Conclusions

The existence of double bonds in the lateral chains incorporated by copolymerisation of ethylene with DMO makes easier the development of crosslinkings after application of irradiation doses. Therefore, at a given dose, the gel content is in the CEDMO copolymer higher than that found in the CEDMO0.0 homopolymer. The different polymeric materials synthesised are semicrystalline and the crystalline characteristics are strongly dependent on composition, mainly from CEDMO0.0 to CEDMO0.7. The importance of comonomer content is in a complete agreement to other results described in the literature for other less bulky comonomeric units: 1-hexene [26], 1-octene [27] and 10-undecenoic acid [28] among others. The effect of irradiation is rather mild in the crystalline features leading to a slight worsening at the highest dose. However, the presence of crosslinkings within amorphous regions allows overcoming those negative aspects and an increase of microhardness, and, consequently, rigidity, is observed in CEDMO0.0, CEDMO0.7 and CEDMO1.0.

Acknowledgements

The authors are grateful for the financial support of Ministerio de Educación y Ciencia (projects MAT2005-00228 and MAT2007 65519-C02-01), Exchange Collaboration Program CSIC/GRICES (projects 2005PT0033 and Proc. 4-1-1 Espanha 2006/2007, respectively), and Fundação para a Ciência e a Tecnologia, Programa Operacional Ciência Tecnologia e Inovação (POCTI) do Quadro Comunitário de Apoio III e comparticipado pelo Fundo Comunitário Europeu FEDER (Project POCTI/CTM/41408/01). The synchrotron work was supported by the European Community-Research Infrastructure Action under the FP6 "Structuring the European Research Area" Programme through the Integrated Infrastructure Initiative "Integrating Activity on Synchrotron and Free Electron Laser Science", contract RII3-CT-2004-506008. We thank the collaboration of the Hasylab personnel, especially Dr S. S. Funari.

References

[1] Khonakdar HA, Jafari SH, Taheri M, Wagenknecht U, Jehnichen D, Haüssler L. J Appl Polym Sci 2006;100:3264–71.
[2] Zhang L, Zhou M, Chen D. Radiat Phys Chem 1994;44:303.
[3] Abou Zeid HM, Ali ZI, Abdel Maksoud TM, Khafagy RM. J Appl Polym Sci 2000;75:179.
[4] Torrisi L, Visco AM, Campo N. J Mater Eng Perform 2007;16:97.
[5] Cartasegna S. Rubber Chem Technol 1986;59:722.
[6] Chodak IJ. Prog Polym Sci 1995;20:1165.
[7] Lazar M, Rado R, Rychlý J. Adv Polym Sci 1990;95:149.
[8] Ratner BD, Hoffman AS, Schoen FJ, Lemons JE. Biomaterials science: an introduction to materials in medicine. San Diego: Academic Press; 1996.
[9] Kaminsky W, Arrowsmith D, Winkelbach HR. Polym Bull 1996;36:577.
[10] Dolatkhani M, Cramail H, Deffieux A. Macromol Chem Phys 1996;197:2481.
[11] Pietikäinen P, Stark P, Seppälä JV. J Polym Sci Part A Polym Chem 1999;37:2379.
[12] Santos JM, Ribeiro MR, Portela MF, Cramail H, Deffieux A. Macromol Chem Phys 2001;202:3043–8.
[13] Santos JM, Ribeiro MR, Portela MF, Cramail H, Deffieux A, Antiñolo A, et al. Macromol Chem Phys 2002;203:139–45.
[14] Cerrada ML, Benavente R, Pérez E, Moniz-Santos J, Ribeiro MR. J Polym Sci Part B Polym Phys 2004;42:3797–808.
[15] Santos JM, Ribeiro MR, Portela MF, Bordado JM. Chem Eng Sci 2001;56:4191–6.
[16] Quinn FA, Mandelkern L. J Am Chem Soc 1958;80:3178.
[17] Wunderlich B. Macromolecular physics, vol. 3. New York: Academic Press; 1980. p. 42.
[18] Baltá-Calleja FJ. Adv Polym Sci 1985;66:117.
[19] Hummel DO, editor. Atlas of polymer and plastics analysis. 2nd ed., vol. 1. Munich: Hanser-Verlig Publishers; 1984.
[20] Bunn CW. Trans Faraday Soc 1939;35:482.
[21] Shirayama K, Kita S-I, Watabe H. Die Makromol Chem 1972;151:97.
[22] Ryan AJ, Stanford JL, Bras W, Nye TMW. Polymer 1997;38:759.
[23] Crist B. J Polym Sci Part B Polym Phys 2001;39:2454.
[24] Cerrada ML, de la Fuente JL, Fernández-García M, Madruga EL. Polymer 2001;42:4647.
[25] Cerrada ML, de la Fuente JL, Madruga EL, Fernández-García M. Polymer 2002;43:2803.
[26] Cerrada ML, Benavente R, Peña B, Pérez E. Polymer 2000;41:5957–65.
[27] Cerrada ML, Benavente R, Pérez E. J Mater Res 2001;16:1103–11.
[28] Cerrada ML, Benavente R, Pérez E, Moniz Santos J, Campos JM, Ribeiro MR. Macromol Chem Phys 2007;208:841–50.